Malaysian Journal of Mathematical Sciences 16(3): 599–623 (2022)
https://doi.org/10.47836/mjms.16.3.12

Malaysian Journal of Mathematical Sciences

Journal homepage: https://einspem.upm.edu.my/journal

Comparative Mathematical Study of Blood Flow Through Stenotic and Aneurysmatic Artery with the Presence and Absence of Blood Clots

Uddin, M. N. *[1], Uddin, M. M.[2], and Alam, M. M.[3]

[1]*Department of Information and Communication Technology, Bangladesh University of Professionals, Dhaka-1216, Bangladesh*
[2]*Department of Mathematics and Physics, North South University, Dhaka-1229, Bangladesh*
[3]*Department of Electrical and Electronic Engineering, Islamic University, Kushtia-7003, Bangladesh*

E-mail: nasiruddin@bup.edu.bd
**Corresponding author*

Received: 26 June 2021
Accepted: 14 July 2022

Abstract

Numerical predictions of blood flow and hemodynamic properties through stenosis and aneurysm artery have been studied in the presence of blood clots at the constricted area. The finite element method has been used to solve the partial differential equations of continuity, momentum, Oldroyd-B, and bioheat transport in cartesian coordinates systems. The present investigation carries the potential to compute blood velocity, pressure, and drag coefficients with significance at the throat of stenosis and aneurysm. The models have also been employed to study simulation, blood clots, and hemodynamic characteristics for all modifications. The impact of shear-thinning on blood flow is intensified compared to the viscoelastic properties. It is found that the maximum effect of the drag coefficient is visible at the hub of stenotic for nonclotting models. The highest pressure and the lowest velocity are gained for the presence of blood clots at the constraint area. The impact of stenosis and aneurysm artery, drag coefficient, and blood clots on blood flow is the main physical outcome that may be reported in medical science to identify atherosclerosis diseases. The quantitative analysis has been completed numerically with the physiological significance of hemodynamic factors of blood flow which shows the validity of the present model.

Keywords: setnotic and aneurysmatic arter; finite element method; cardiovascular disease; blood clots.

1 Introduction

The cardiovascular system of the human body is affected due to irregular cell increases or decreases in blood vessels which leads to arterial diseases in various organs. Although it is not clearly identified of exact mechanisms for inventing this matter. It's been found that blood flow disorders, initiation of arterial diseases and irregularities have been created from mild stenosis [31, 38]. A good number of researchers are continuing studies to understand stenotic blood flow experimentally, theoretically, and numerically. Smith [56] has details studied of steady flow through an axisymmetric stenosis artery and shown that blood flow strongly depends on the stenotic geometry condition. The real understanding of the blood pulsatile flow cannot be ignored. Many researchers have completed their studies with laboratory-based, theoretically, and computationally on blood flow at stenotic conditions for Newtonian fluid [9, 32, 39, 14, 15]. It is very important that blood flow obeys Newtonian law for high shear rate flow. In case of a low shear rate, the fluid behavior will be non-Newtonian, especially if the blood flow is in smaller arteries and the down steam of the stenosis. It has been pointed out that blood shows non-Newtonian performances (Thixotropy, Viscoelasticity, and Shear-thinning) for cardiovascular diseases. Recently, researchers [34] have been given more concentrations for non-Newtonian blood flow analysis with various stenosis conditions and still have a lot of scopes to work in this area.

In this paper, we have also considered the aneurysm condition of blood vessels. It is another severe situation that about 75 percent of all patients have died before reaching the hospital, and it is an extreme risk for the human body [36]. Ingoldby et al. [26] have shown that when these prehospital deaths are counted, the overall mortality rate may exceed 90 percent. Ernst [18] has studied the increasing median age of the population contributes to increasing incidence. It is important to identify the risk features that may play a key role in aneurysm growth and rupture, which have become a unified multidisciplinary task to a clear understanding of the pathogenesis and growth of aneurysms. Numerical and experimental studies have been performed to interpret blood flow through aneurysmatic artery during the last and present decades [60, 16, 55] and biomechanics has been receiving the attention of researchers in this area and providing numerical solutions of human blood flow systems in various conditions [13]. In most of the inquiries, flow is considered in cylindrical pipes with uniform cross-section areas. But it is well known that blood vessels deform at the change of bone shape for various reasons in the human body. Hence, the idea of blood flow in various cross-sections forms the prime basis of a large class of problems in understanding blood flow patterns. Most of the studies have considered long, narrow and tapering vessels for blood flow analysis [44, 35, 22] of Newtonian and non-Newtonian cases. Thus, the effects of stenotic and aneurysmatic vessels with the non-Newtonian performance of the flowing blood seem to be identically significant and hence definitely deserve special consideration.

Recently, it is found that the classical Newtonian fluids are not appropriate to illustrate the physiological fluids in the human organ. The fluid of the human body has exhibited more sophisticated behaviors due to the viscoelasticity, shear thinning, shear thickening, and memory effects. So, it is very difficult to predict all their non-Newtonian characteristics due to the complexity in the rheology of various body materials. Hence, various models are used to describe the appropriate functionality of rheological features of human blood fluids [54, 27, 50]. The Oldroyd-B, a non-Newtonian fluid, is used to describe the viscoelastic properties of physiological fluids [41, 46, 20]. Some physical applications of this fluid are chemical processing (polymers), biological materials (blood), plastics manufacturing industry, mining processing industry, oiling industry, biofluid, viscoelastic fluids like paints, honey, toothpaste, DNA suspensions, and the chemical industry of shampoo and creams, etc. In general, these fluids show certain different features such as viscosity, viscoelasticity, viscoelasticity, history effects, etc. [65].

Therefore, we are motivated by the mathematical study of blood flow through stenotic and aneurysmatic arteries with blood clots. Thus, an effort is made in the present theoretical study to develop a mathematical model and numerical analysis in order to investigate the significant characteristics of the blood flow through a rigid stenotic and aneurysmatic vessel. The generalized cross model has been used to analyze the non-Newtonian behaviour of flowing blood flow. Malek et al. [33, 54] have widely studied the existence and uniqueness, as well as the stability characteristics of streaming flow problems. The present problem is one of the major physiological significance, due attention is also paid to comparable studies in the presence of blood clots and without blood clots for the considered model.

The novelty of this work is to identify the atherosclerosis diseases in case of blood clots and stenotic (without blood clots) conditions by drag coefficient. The drag coefficient value indicates the existence of a stenotic artery, and the maximum value is found in the generalized Oldroyd-B case. It is another finding that the recirculation zones are more prominent at the throat of the stenotic artery compared to the blood clot area. A theoretical correlation has been found between velocity and pressure for all models. Due to the presence of blood clots at the stenosis artery, the blood flow pattern has been affected significantly. The impact of the stenotic region or aneurysmatic artery leads to identifying arterial diseases. The effect of the drag coefficient on the blood flow is an important factor in the onset of vascular diseases which is the uniqueness of the study. We have used the following notations which are available in mathematical structures. The dimensionless numbers Weissenberg number, Reynolds number and Prandtl number are denoted by *Wi*, *Re*, *Pr* respectively, sigma denotes stress tensor and *P* is the pressure. The velocity components are U and V along with X and Y respectively. The perfusion coefficient is visco-elasticity components, and the heat source is denoted by Q. The frequently used nomenclature in this paper is summarized in Table 1.

Table 1: The frequently used nomenclature.

σ	Stress Tensor (Pa)	μ_n	Polymer viscosity
σ_v	Viscous stress tensor (Pa)	μ_s	Solvent viscosity
σ_n	Solvent stress tensor (Pa)	$V^/$	Anti-symmetry velocity gradient
L	height	$\dot{\gamma}$	Rate of deformation tensor
I	Identity matrix	u, v	velocity components (ms-1)
Wi	Weissenberg number	U,V	Dimensionless velocity components
p	pressure (Nm^-2)		**Greek symbols**
P	non-dimensional pressure	μ	Viscosity (N s m^{-2})
Re	Reynold number	γ	Deformation tensor
q	Flow rate (m^2/s)	ρ	density of the fluid (kgm^-3)
λ_x	Relaxation time	υ	kinematic viscosity of the fluid $(m^2)(s^-1)$
λ_d	Retardation time	τ_s	Extra-stress tensor (N/m^2)
V	Symmetry velocity gradient		

2 Preliminaries

This section briefly reviews some fundamental concepts from previous works of literature. The goal is to establish some notations and results that will be used in the later section of this paper.

Since the invention of stenosis or aneurysm effect on blood flow in our human arteries has created serious disorders in the circulatory system that lead to various cardiovascular diseases such as arteriosclerosis, bleeding, stroke, kidney damage, etc. [28,29]. At present, medical researchers, bioengineers and numerical scientists join efforts to provide numerical simulations of human blood flow systems under different conditions. The exchange of knowledge and data information is the core purpose of this kind of collaboration that can be used in simulations. A

relation has been established by Thurston [59] between blood shear rate and the viscoelasticity of blood flow. Firstly, Wille [64] has described the numerical study of pulsatile blood flow through aneurysms vessels and shown the existence of vortex of various sizes during the cardiac cycle. Oka [40] has studied a taper analysis of blood flow to identify arterial disease, and shown pressure development is a vital factor in atherosclerosis diseases. Kumar et al. [30] have explained the pulsatile suspension flow in a dilated blood vessel. They have determined the additional complications of hemodynamics in diseased arterial vessels having an aneurysm and stenosis artery.

During the blood circulation system, the hemodynamic features of blood can play a vital role in developing severe cardiovascular diseases. Anand et al.[7] have described a model for blood flow simulation with Oldroyd-B fluid properties. They have [6, 47] also exposed a model with blood clots for the formation and analysis. Shih et al. [53] have studied on skin surfaces with sinusoidal heat flux conditions. A thermodynamic framework has been studied by Rajagopal and Srinivasa [47] to show the blood viscoelastic response with various configurations. With the presence of hematocrit in a local aneurysm, the systematic analysis of flow features through a tube and artery has been studied by Mukhopadhyay and Layek [36]. Prokop and Kozel [45] have shown a numerical simulation of generalized Newtonian and Oldroyd-B fluids with an extended computation domain. Nadeem et al. [38] have shown the reduction of wall shear stress and resistance impedance to blood flow with the influence of metallic nanoparticles.

Akbar et. al. [67] have analyzed the slip effects on unsteady non-Newtonian blood flow having an inclined catheterized overlapping stenotic artery. They [66] have also discussed a theoretical study of an unsteady two-layered blood flow through a w-shaped stenosed artery using generalized Oldroyd-B fluid. The pulsatile blood flow has been described by Achab et al. [3] to evaluate the blood flow characteristics and the wall shear stress under physiological conditions through a stenosis artery. Magnetohydrodynamics (MHD) thin-film flow and thermal analysis of blood with CNTs nanofluid have been studied by Alsagri et. al [5]. Zahir shah et. al. [52] have discussed the micropolar gold blood nanofluid flow and radiative heat transfer between permeable channels. Nasir and Alim [61] have described blood flow through stenotic arteries with various flow rates numerically. Later, they [62] have also demonstrated numerical investigation of blood flow through a double stenotic artery. Zhang et. al. [71] have studied an entropy analysis on the blood flow using nanoparticles for tapered arteries. Bhatti et. al. [10] have studied the mass transfer biologically on the rheology for Williamson nanofluid flow under convection with magnetic impacts. The Mathematical analysis has been discussed for blood flow through a bifurcated artery by Rajasekhar et. al [48] using the finite element method.

Recently, Akbar et. al. [69] have discussed the effects of nanoparticles on unsteady blood flow through stenosed vessels and determined numerically. A biomedical study of nanoparticles on unsteady blood flow through a catheterized stenotic vessel has been analyzed by the same authors [70]. Soon after that, Akbar and Ambreen [68] studied the curvature effects on nano-fluid flow in a w-shape stenosed channel with time-dependent. Hoque et. al [25] have detected the severity of atherosclerotic for single and multiple stenoses in a coronary artery.

A large-scale numerical analysis has been carried out by performing mathematical computations of the desired quantities having more physiological significance to explore the effect of the stenotic vessel, aneurysmatic artery, blood clots, drag coefficient, and dimensionless numbers. The non-Newtonian behaviour of the streaming blood on the physiological flow phenomena, which are extensively quantified through their graphical representations are presented in the result section with appropriate scientific discussion. A comparative study has been exposed in the presence of blood clots and without blood clots to know the significances of coagulation blood. Code validation results are also shown with Prokop et. al. [45] to authenticate the applicability of the present study.

3 Modeling and Analysis of Blood Flow

This section contains the main results of this paper. At first, we have specified the physical model. Then formulate the mathematical model using partial differential equations (PDE) with its boundary conditions. Finally, a numerical technique has been discussed to solve the mathematical model efficiently.

3.1 Model Specifications

The treated model is a two-dimensional rigid artery with stenosis and aneurysm vessel wall in a cartesian system. The considered model in the present study is displayed in Figure 1. Figures 2 and 3 are the focal motivations for considering the present model. The model is considered with stenosis and aneurysmal heights $h_s = R$ and $h_a = 3R$. The upper and bottom stenosed vessel walls are cool (T_c) and heated (T_h), while the rest of the walls are adiabatic and impermeable with no-slip conditions. The velocity profile and the pressure are prescribed at entrance and departure respectively. Blood flow acceleration is expected at stenotic and aneurysmatic cross-sectional areas. A mathematical structure has been used by Achab et. al. [3] with cosine shaped for the stenosis model. The modified mathematical model of physical construction in the presence of stenosis and aneurysm is in cosine shape as follows:

$$y = \left\{ \begin{array}{c} 0.5D\ \left[1 - \frac{\varepsilon}{D}\left(1 + cos\pi\ M(x)\right)\right]; 0 \leq x \leq L_s \\ 0.5D\ \left[1 + \frac{\varepsilon}{D}\left(1 + cos\pi\ N(x)\right)\right]; L_s < x \leq L_a \\ 1 \qquad\qquad\qquad\qquad\qquad ; Otherwise \end{array} \right\};$$

where $M\left(x\right) = x - \frac{x_s}{L}$ and $N\left(x\right) = x - \frac{x_a}{L}$, x_s and x_a are the centers of stenosis and aneurysm respectively, L is the length of stenosis and aneurysm, ε is the maximum height of stenosis and aneurysm, the model diameter, D=2R, the location of stenosis, L_s = 3R, the position of aneurysm L_a= 3R, total model length is 10R and R=3.1.

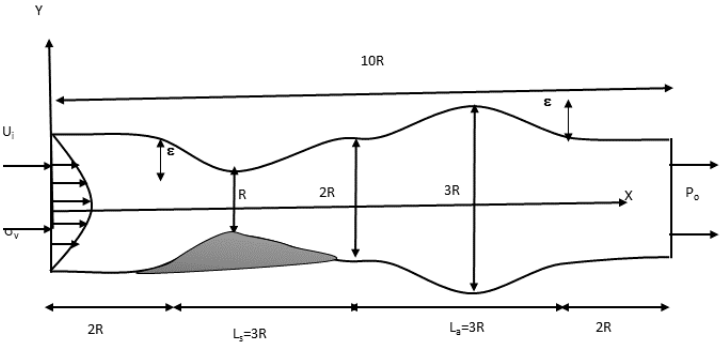

Figure 1: Structure of the computational domain.

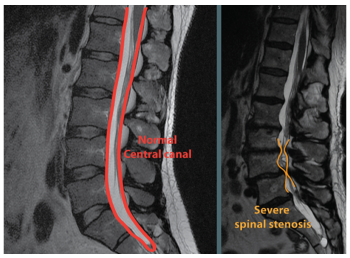

Figure 2: View of severe spinal stenosis [2].

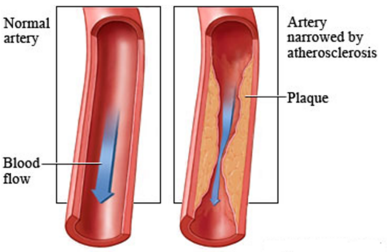

Figure 3: View of development of plaque [**?**].

3.2 Mathematical Model

The functioning fluid is assumed to be laminar blood flow and incompressible with shear-thinning and viscoelasticity properties. The generalized Oldroyd-B model is used to capture non-Newtonian properties of blood flow. The leading mathematical equations of the conservation of mase (continuity equation), momentum equation (Navier Stokes equation) [11, 19] Oldroyd-B constitutive equation [42] and bio-heat equation [43] for steady-state blood flow is given below: Continuity Equation:

$$\nabla.\,\mathbf{u} = 0 \tag{1}$$

Momentum Equation:

$$\rho\frac{\partial \mathbf{u}}{\partial t} + \rho(\mathbf{u}.\nabla)\mathbf{u} = -\nabla \mathrm{p} + \mu_n \Delta \mathbf{u} + \nabla.\sigma + \rho f \tag{2}$$

$$\rho\frac{\partial \mathbf{v}}{\partial t} + \rho(\mathbf{v}.\nabla)\mathbf{v} = -\nabla \mathrm{p} + \mu_n \Delta \mathbf{v} + \nabla.\sigma + \rho f \tag{3}$$

Oldroyd-B Constitutive Equation:

$$\sigma + \lambda_x[\frac{\partial \sigma}{\partial t} + (\mathbf{u}.\nabla)\sigma] = 2\nabla_v \mathbf{V(u)} + \lambda_x[\sigma V' - V'\sigma - \sigma V - V\sigma] \tag{4}$$

Bio-heat Equation:

$$\rho c_p[\frac{\partial T}{\partial t} + (\mathbf{u}.\nabla)T] = K\nabla^2 T + q + \rho_b c_b w_b(T_b - T) \tag{5}$$

Here, $\mathbf{u} = (u_1, u_2, u_3)^T$ is the velocity vector, ρ is constant density, $\boldsymbol{\sigma}$ = -pI+2μ_n**V**+**T** is total stress tensor, $\mu = \mu_v + \mu_n$. is dynamic viscosity, λ_x denotes relaxation time, **T** is extra stress tensor, p is pressure, the symmetric part of the velocity gradient, $\mathbf{V} = \frac{1}{2}(\nabla \mathrm{u} + \nabla u^T)$ i.e. $\sigma = 2\mu V$, ρ_b is blood density, T_b is arterial blood temperature, w_b is blood perfusion rate, c_b is specific heat capacity of blood, c_p is tissue specific heat and heat source, q = q_m + q_g, where q_m denotes the metabolic heat generation and q_g is the volumetric heat generation due to the nanoparticles. We can write $\boldsymbol{\sigma} = \boldsymbol{\sigma}_n + \boldsymbol{\sigma}_v$; where the Newtonian stress tensor is given by $\boldsymbol{\sigma}_n = 2\mu_n \mathbf{V}$, and viscoelastic of stress tensor is $\boldsymbol{\sigma}_v + \lambda_x \frac{\delta \boldsymbol{\sigma}_v}{\delta t} = 2\mu_v \mathbf{V}$, the dynamic viscosity, $\mu = \mu_n + \mu_v$ and $\frac{\lambda_d}{\lambda_x} = \frac{\mu_n}{\mu_n + \mu_v}$.

The mathematical model can be written as follows for the general quantity **N**,

$$\frac{\delta \mathrm{N}}{\delta \mathrm{t}} = \frac{\partial N}{\partial t} + (\mathrm{u}.\nabla)N) - (V'N - NV') - (VN + NV),$$

where the velocity gradient for symmetric part is given by:

$$V = \frac{1}{2}(\nabla \mathrm{u} + \nabla u^T) = \frac{1}{2}\begin{pmatrix} 2\mathrm{u}_x & u_y + v_x \\ u_y + v_x & 2\mathrm{v}_y \end{pmatrix},$$

and velocity gradient for anti-symmetric part is given by:

$$V' = \frac{1}{2}(\nabla \mathrm{u} - \nabla u^T) = \frac{1}{2}\begin{pmatrix} 2\mathrm{u}_x & u_y - v_x \\ u_y - v_x & 2\mathrm{v}_y \end{pmatrix}.$$

Meanwhile, the Oldroyd-B equation is given by:

$$\frac{\partial T_v}{\partial t} + (u.\nabla)T_v = \frac{2\mu_v}{\lambda_x}V - \frac{1}{\lambda_x}T_v + (V'T_v - T_vV') + (\mathrm{V}Tv + TvV).$$

The shear-thinning manners for blood flow is viscosity function $\mu(\dot{\gamma})$ which is dependent on the shear rate, $\dot{\gamma} = 2|\mathbf{V}|$. The dimensionless form of the viscosity function is

$$f(\dot{\gamma}) = \frac{\mu(\dot{\gamma}) - \mu_\infty}{(\mu_0 - \mu_\infty)}.$$

Where, μ_0 is the asymptotic viscosity values at zero and μ_∞ is infinite shear rates. The viscosity function is satisfied for the following conditions

$$\lim_{\hat{i}\to 0^+} F(\gamma) = 1 \quad \text{and} \quad \lim_{\hat{i}\to\infty} .F(\gamma) = 0.$$

We have selected the blood viscosity function f($\dot{\gamma}$) among many functions to get blood flow simulations accurately. The generalized Cross model [51, 21] is used to analysis the blood shear-thinning which is denoted by

$$\mu(\dot{\gamma}) = \mu_\infty + \frac{\mu_0 - \mu_\infty}{(1 + (\lambda\dot{\gamma})^b)^a} \text{ with the parameters a, b ,} \lambda > 0.$$

The following dimensionless quantities are used to dimensionless the above leading partial differential equations:
$x = LX, y = LY, t = Lt^*/U, \boldsymbol{u} = UU_o, \boldsymbol{v} = VU_o p = \mu UP/L, \sigma = U\mu\sigma^*/L, f = f^*\mu U/L^2,$
$\nabla = \nabla^*/L, Wi = \lambda_x U/L, Re = \rho UL/\mu, P_r = \mu c_p/k, \theta = k\,(T - T_c)\,/qL^2, q = Qq_0,$
$w_b = \rho_f k/\rho c_b L^2,$
where the dimensionless quantities X and Y are the coordinates varying along horizontal and vertical directions respectively. U and V are velocity components along X and Y axes respectively, P is pressure, L is characteristics length, σ* denotes stress tensor, Q is heat source, ρ_f is perfusion coefficient, and Weissenberg number (Wi), Reynold number (Re), Prandtl number (Pr) are dimensionless numbers.

By using the above non-dimensional scale variables, the dimensionless partial differential equations 6 , 7, 8, 9 are obtained in vector form for 2D stenosis and aneurysmal vessel in domain Ω as follows:
Continuity Equation:

$$\nabla.\,\mathbf{U} = 0. \tag{6}$$

Momentum Equations:

$$Re[(\mathbf{U}.\ \nabla)\{\mathbf{U}] = -\nabla P + (1-\lambda)\boldsymbol{\Delta}\mathbf{U} + \nabla.\boldsymbol{\sigma} + f \tag{7}$$

$$Re[(\mathbf{V}.\ \nabla)\mathbf{V}] = -\nabla P + (1-\lambda)\boldsymbol{\Delta}\mathbf{V} + \nabla.\boldsymbol{\sigma} + f. \tag{8}$$

Oldroyd-B constitutive equation:

$$W_i[(\mathbf{U}.\nabla)\boldsymbol{\sigma}] + \boldsymbol{\sigma} = 2\mu_v\mathbf{V}(\mathbf{U}) + W_i[(\nabla\mathbf{U})\boldsymbol{\sigma} + \boldsymbol{\sigma}(\nabla\mathbf{U})^t]. \tag{9}$$

Bio-heat Equation:

$$RePr(\mathbf{U}.\nabla)\theta = \nabla^2\theta + \mathrm{Q} - \rho_f\theta. \tag{10}$$

3.2.1 Boundary Conditions

In the present study the blood clot, outlet, inlet and rigid wall are four distinct parts of the model and the boundary settings are essential to solve the governing partial differential equations. The boundary conditions for present problem are specified as follows:
(i) At inlet:
It is required to prescribe either Dirichlet (velocity) or Neumann (surface force) boundary conditions [45] at the inlet to develop parabolic velocity profile due to insufficient physiological data. The axial velocity profile and the corresponding extra stresses components [12] are
$u = 1.5U_i(1-y^2), v = 0$
$\sigma_{11} = 2\mu_v Wi(\frac{\partial u}{\partial y})^2,\ \ \sigma_{12} = \mu_v\ \frac{\partial u}{\partial y}, \sigma_{22} = 0;$
where y is along the inlet boundary, and the mean fluid velocity at the inlet is U_i
(ii) At outlet:
a. At outlet homogeneous Neumann conditions are used for the velocity components and a constant pressure are prescribed.
b. Due to pressure force (P_o) the stress is acting at the boundary, σ, $\mathbf{n} = -P_o\mathbf{n}$
(iii) At boundary wall:
a. The velocity, $\mathbf{u}$= 0 and the normal component of the extra stress, $(\boldsymbol{\sigma}.\ \mathbf{n}).\ \mathbf{n} = 0$ are considered on the artery wall.
b. Neumann boundary conditions are applied at the artery wall for the pressure.
(iv) At stenosed wall:
The blood clotted wall are heated and the upper wall is cooled at the stenotic area for the present model.

In this work, the continuity equation 6, momentum equations 7,8, Oldroyd-B equation 9, and bio-heat equation 10 are considered to account for blood viscoelasticity. The following models

are tested and shown in Table 2 for different flow rates ($q = 0.05, 0.1, 2cm^3/\text{ s}$), that correspond to the common blood flow rates in the human body for the combination of shear-thinning and viscoelasticity.

Table 2: Model's framework.

Model's Name	**Shear-thinning** (μ_n)	**Viscoelasticity** (σ_v)
1. Newtonian (N)	$\mu_n = \mu_\infty =$ constant	$\boldsymbol{\sigma}_v$ =0
2. Generalized Newtonian (GN)	$\mu_n = \mu(\dot{\gamma})$	$\boldsymbol{\sigma}_v$ =0
3. Oldroyd-B(OD)	$\mu_n = \mu_\infty =$ constant	$\boldsymbol{\sigma}_v$
4. Generalized Oldroyd-B (GD)	$\mu_n = \mu(\dot{\gamma})$	$\boldsymbol{\sigma}_v$

3.3 Numerical Analysis

Galerking weighted residual finite techniques are applied to solve the governing partial differential equations numerically. The finite element methods is described in details by Zienkiewicz and Taylor [72] and Dechaumphai [17]. The numerical solution of the current study is discussed in Section-3.3.3.

3.3.1 Mesh Generation

The mesh creation is an essential part in finite element procedure. An unstructured grid can be formed for the governing equations, and it may be written in integral form. numerical integration can be carried out precisely without coordinate transformation on the unstructured grid domain. A triangular mesh generation is shown in Figure 4 in 2D domain. In the technique, the meshing is a process to sub-divide of a continuous geometry into a set of sub-domains. In the Figure 4, a domain (Ω) is split into a set of sub-domains, Ω^e with edge Γ^e. A mesh structures of the present model is demonstrated in Figure 5.

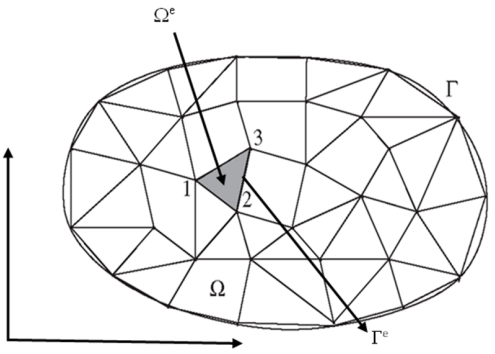

Figure 4: A triangular mesh generation of a domain [49].

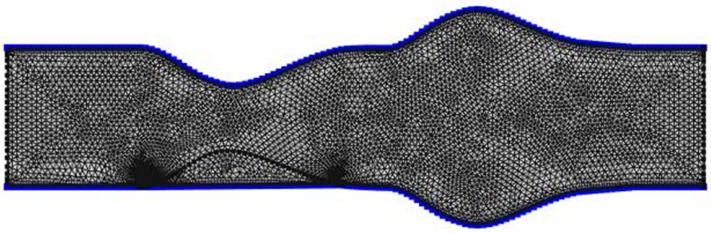

Figure 5: Mesh generation of stenotic and aneurysmatic artery.

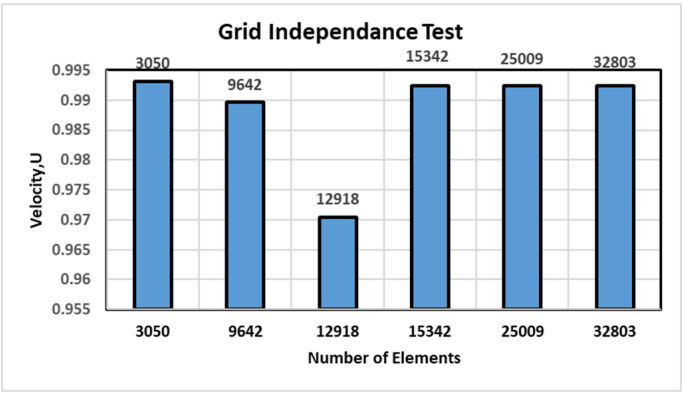

Figure 6: Convergence of mean velocity for Re = 10^3, and Wi = 0.6 with $q = 0.1cm^3$/s.

3.3.2 Grid Sensitivity Test

A grid independence test are used to select the suitable grid size for the present study with Re=1000,W_i=0.5 and q = $0.1cm^3$/s. In the case of generalized Newtonian model, the convergence of the velocity with refinement are shown in Figure 6. The grid sensitivity test is performed for six different types of meshes. The mean blood velocity is used as sensitivity measures of the accuracy of the result. In this study, 25009 meshes are carried out for numerical correctness.

3.3.3 Numerical Solutions

The discretized momentum and Oldroyd-B equations subjected to the boundary conditions simultaneously will be solved using the Matlab programming [29] & Mathematical programming

package COMSOLMULTIPHYSICS [1] for the dependent variables (velocity, pressure and stress tensor). So we first solve the velocity from equations 6, 7, 8 and 9 and then compute the pressure using $p = 2\mu_s \mathbf{V}(u) + T + \sigma$. The numerical procedure [58] have been used in this work based on the Galerkin-weighted residual method of finite element formulation and details are given here below. After the applying the weighted residual method then

$$\int_A N_\alpha (\nabla.U)\mathrm{dA} = 0, \tag{11}$$

$$Re \int_A N_\alpha U(\nabla \cdot U)dA = -\int_A H_\lambda \nabla P dA + \int_A N_\alpha \nabla \sigma dA + (1-\lambda)\int_A N_\alpha \nabla^2 U dA + \int_A N_\alpha f dA, \tag{12}$$

$$Re \int_A N_\alpha U(\nabla \cdot V)dA = -\int_A H_\lambda \nabla P dA + \int_A N_\alpha \nabla \sigma dA + (1-\lambda)\int_A N_\alpha \nabla^2 V dA + \int_A N_\alpha f dA, \tag{13}$$

$$W_i \int_A N_\alpha U(\nabla.\sigma)dA + \int_A N_\alpha \sigma dA = \int_A \mu_\nu N_\alpha((\nabla.U)dA + W_i \int_A N_\alpha U(\nabla.U)\sigma + \sigma(\nabla.U)dA, \tag{14}$$

$$RePr \int_A N_\alpha (U.\nabla)\theta dA = \int_A N_\alpha \nabla^2 \theta dA + \int_A N_\alpha Q dA - \int_A N_\alpha \rho_f \theta dA. \tag{15}$$

To generate the boundary integral terms associated with the surface tractions, extra-stress tensor and temperature the Equations 11, 12, 13, 14, 15 become after applying Gauss's theorem.

$$Re \int_A N_\alpha U(\nabla.U)dA + \int_A H_\lambda \nabla P dA - \int_A N_\alpha \nabla \cdot \sigma dA - (1-\lambda)\int_A N_\alpha \nabla^2 U dA - \int_A N_\alpha f_x dA = \int_{s_0} N_\alpha S_x ds_0, \tag{16}$$

$$Re \int_A N_\alpha U(\nabla.V)dA + \int_A H_\lambda \nabla \mathrm{P} dA - \int_A N_\alpha \nabla \sigma dA - (1-\lambda)\int_A N_\alpha \nabla^2 V dA - \int_A N_\alpha f_y dA = \int_{s_0} N_\alpha S_y ds_0, \tag{17}$$

$$W_i \int_A N_\alpha U \cdot (\nabla\sigma)\mathrm{dA} + \int_A N_\alpha \sigma \mathrm{dA} - \int_A \mu_v N_\alpha \nabla \cdot U \mathrm{dA} - W_i \int_A N_\alpha [(\nabla \cdot U)\sigma + \sigma(\nabla \cdot U)]\mathrm{dA} = \int_A N_\alpha \sigma_w \mathrm{ds}_w, \tag{18}$$

$$RePr\int_A N_\alpha(U.\nabla)\theta dA - \int_A N_\alpha\nabla^2\theta dA - \int_A N_\alpha Q dA + \int_A N_\alpha\rho_f\theta dA = \int_{s_w} N_\alpha q_w ds_w. \tag{19}$$

Here, Equations 16, 17 specify surface tractions (S_x, S_y) along the outflow boundary S_0, Equations 18, 19 specify velocity components, stress tensors and fluid temperatures that can be applied force from the domain along wall boundary S_w. The six-node triangular element is used for the development of finite element equations. All six nodes are associated with velocities, temperature, as well as stress tensors; only the corner nodes are associated with pressure. This means that a lower-order polynomial is chosen for pressure, and which is satisfied through continuity equation. The basic unknowns for the above differential equations are the velocity components U, V the stress tensor, σ and the pressure, P. The velocity component and the stress tensor distributions and linear interpolation for the pressure distribution according to their highest derivative orders in the differential Equations 6, 7, 8 9, 10 as

$$U(X,Y) = N_\alpha U_\alpha, \tag{20}$$

$$V(X,Y) = N_\alpha V_\alpha, \tag{21}$$

$$\sigma(X,Y) = N_\alpha \sigma_\alpha, \tag{22}$$

$$P(X,Y) = H_\lambda P_\lambda, \tag{23}$$

$$\theta(X,Y) = N_\alpha \theta_\alpha, \tag{24}$$

where $\alpha = 1, 2, ..., 6$; $\lambda = 1, 2, 3$; Nα are the element interpolation functions for the velocity components and the stress tensor, and Hλ are the element interpolation functions for the pressure. Substituting the element velocity component distributions, the stress tensor distribution, and the pressure distribution from Equations 6, 7, 8, 9, 10 the finite element equations can be written in the form,

$$K_{\alpha\beta^x}U_\beta + K_{\alpha\beta^y}V_\beta = 0, \tag{25}$$

$$\begin{aligned} &Re(K_{\alpha\beta\gamma^x}U_\beta U_\gamma + K_{\alpha\beta\gamma^y}V_\beta U_\gamma) + M_{\alpha\mu^x}P\mu + K_{\alpha\beta^x}\sigma_\beta + \\ &K_{\alpha\beta^y}\sigma_\beta + (1-\lambda)(S_{\alpha\beta^{xx}} + S_{\alpha\beta^{yy}})U_\beta - f_x K_\alpha = Q_{\alpha^u}, \end{aligned} \tag{26}$$

$$Re(K_{\alpha\beta\gamma^x}U_\beta V_\gamma + K_{\alpha\beta\gamma^y}V_\beta V_\gamma) + M_{\alpha\mu^y}P_\mu + K_{\alpha\beta^x}\sigma_\beta + K_{\alpha\beta^y}\sigma_\beta + (1-\lambda)(S_{\alpha\beta^{xx}} + S_{\alpha\beta^{yy}})V_\beta - f_y K_\alpha = Q_{\alpha^v}, \tag{27}$$

$$W_i(K_{\alpha\beta\gamma^x}U_\beta\sigma_\gamma + K_{\alpha\beta\gamma^y}V_\beta\sigma_\gamma) + K_{\alpha\beta}\sigma_\mu - \mu_v(K_{\alpha\beta^x}U_\alpha + K_{\alpha\beta^y}U_\beta) - W_i\,(K_{\alpha\beta\gamma^x}U_\beta\sigma_\gamma + K_{\alpha\beta\gamma^y}U_\beta\sigma_\gamma) = Q_{\alpha^T}, \tag{28}$$

$$RePr(K_{\alpha\beta\gamma^x}U_\beta\theta_\gamma + K_{\alpha\beta\gamma^y}V_\beta\theta_\gamma) + (S_{\alpha\beta^{xx}} + S_{\alpha\beta^{yy}})\theta_\beta - K_\alpha Q + \rho_f K_{\alpha\beta}\theta_\beta = Q_{\alpha^\theta}, \tag{29}$$

where the coefficients in element matrices are in the form of the integrals over the element area and along the element edges S_0 and S_w as,
$K_\alpha = \int_A N_\alpha dA$,
$K_{\alpha\beta^x} = \int_A N_\alpha N_{\beta,x} dA$,
$K_{\alpha\beta^y} = \int_A N_\alpha N_{\beta,y} dA$,
$K_{\alpha\beta\gamma^x} = \int_A N_\alpha N_\beta N_{\gamma,x} dA$,
$K_{\alpha\beta\gamma^y} = \int_A N_\alpha N_\beta N_{\gamma,y} dA$,
$K_{\alpha\beta} = \int_A N_\alpha N_\beta dA$,
$S_{\alpha\beta^{xx}} = \int_A N_{\alpha,x} N_{\beta,x} dA$,
$S_{\alpha\beta^{yy}} = \int_A N_{\alpha,y} N_{\beta,y} dA$,
$M_{\alpha\mu^x} = \int_A H_\alpha H_{\mu,x} dA$,
$M_{\alpha\mu^y} = \int_A H_\alpha H_{\mu,y} dA$,
$Q_{\alpha^u} = \int_{S_0} N_\alpha S_x dS_0$,
$Q_{\alpha^v} = \int_{S_0} N_\alpha S_y dS_0$,
$Q_{\alpha^\sigma} = \int_{S_0} N_\alpha \sigma_w dS_w$,
$Q_\alpha\theta = \int_{S_w} N_\alpha q_w dS_w$.

By using the Newton-Raphson iteration technique, the set of nonlinear algebraic Equations 25, 26, 27, 28, 29 are transferred into linear algebraic equations. Finally, these linear equations are solved by applying the triangular factorization method and reduced integration technique of Zeinkiewicz and Taylor [60] and the finite element Equations 25, 26, 27, 28, 29 as,

$$F_{\alpha^p} = K_{\alpha\beta^x}U_\beta + K_{\alpha\beta^y}V_\beta, \tag{30}$$

$$F_{\alpha^u} = Re(K_{\alpha\beta\gamma^x}U_\beta U_\gamma + K_{\alpha\beta\gamma^y}V_\beta U_\gamma) + M_{\alpha\mu^x}P\mu - K_{\alpha\beta^x}\sigma_\beta - K_{\alpha\beta^y}\sigma_\beta + (1-\lambda)(S_{\alpha\beta^{xx}} + S_{\alpha\beta^{yy}})U_\beta - f_x K_\alpha - Q_{\alpha^u}, \tag{31}$$

$$F_{\alpha^v} = Re(K_{\alpha\beta\gamma^x}U_\beta V_\gamma + K_{\alpha\beta\gamma^y}V_\beta V_\gamma) + M_{\alpha\mu^y}P_\mu - K_{\alpha\beta^x}\sigma_\beta - K_{\alpha\beta^y}\sigma_\beta + (1-\lambda)(S_{\alpha\beta^{xx}} + S_{\alpha\beta^{yy}})V_\beta - f_y K_\alpha - Q_{\alpha^v}, \tag{32}$$

$$F_{\alpha^\sigma} = W_i(K_{\alpha\beta\gamma^x}U_\beta\sigma_\gamma + K_{\alpha\beta\gamma^y}V_\beta\sigma_\gamma) + K_{\alpha\beta}\sigma_\beta - \mu_v(K_{\alpha\beta^x}U_\beta + K_{\alpha\beta^y}V_\beta) - 2W_i\,(K_{\alpha\beta\gamma^x}U_\gamma\sigma_\beta + K_{\alpha\beta\gamma^y}U_\gamma\sigma_\beta) - Q_{\alpha^\sigma}, \tag{33}$$

$$F_{\alpha^\theta} = RePr(K_{\alpha\beta\gamma^x}U_\beta\theta_\gamma + K_{\alpha\beta\gamma^y}V_\beta\theta_\gamma) + (S_{\alpha\beta^{xx}} + S_{\alpha\beta^{yy}})\theta_\beta - K_\alpha Q + \rho_f K_{\alpha\beta}\theta_\beta - Q_{\alpha^\theta}. \tag{34}$$

This leads to a set of algebraic equations with the incremental unknowns of the element's nodal velocity components, temperatures, and pressures in the form,

$$\begin{bmatrix} K_{uu} & K_{uv} & K_{u\sigma} & K_{u\theta} & K_{up} \\ K_{vu} & K_{vv} & K_{v\sigma} & K_{v\theta} & K_{vp} \\ K_{\sigma u} & K_{\sigma v} & K_{\sigma\sigma} & 0 & 0 \\ K_{\theta u} & K_{\theta v} & 0 & K_{\theta\theta} & 0 \\ K_{pu} & K_{pv} & 0 & 0 & 0 \end{bmatrix} \begin{Bmatrix} \Delta u \\ \Delta v \\ \Delta\sigma \\ \Delta\theta \\ \Delta p \end{Bmatrix} = - \begin{Bmatrix} F_{\alpha^u} \\ F_{\alpha^v} \\ F_{\alpha\sigma} \\ F_{\alpha^\theta} \\ F_{\alpha^p} \end{Bmatrix}, \tag{35}$$

where

$K_{uu} = Re(K_{\alpha\beta\gamma^x}U_\gamma + K_{\alpha\gamma\beta^x}U_\gamma + K_{\alpha\beta\gamma^y}V_\beta) + (1-\lambda)\,(S_{\alpha\beta^{xx}} + S_{\alpha\beta^{yy}})\,,$
$K_{uv} = K_{\alpha\beta\gamma^y}U\gamma, K_{uT} = -K_{\alpha\beta^x} - K_{\alpha\beta^y}, K_{up} = M_{\alpha\mu^x}K_{vu} = K_{\alpha\beta\gamma^x}V\gamma,$
$K_{vv} = Re(K_{\alpha\beta\gamma^x}U_\beta + K_{\alpha\gamma\beta^x}V_\gamma + K_{\alpha\gamma\beta^y}V_\gamma) + (1-\lambda)\,(S_{\alpha\beta^{xx}} + S_{\alpha\beta^{yy}})\,,$
$K_{v\sigma} = -K_{\alpha\beta^x} - K_{\alpha\beta^y}\,,\quad K_{vp} = M_{\alpha\mu^y},\quad K_{\sigma u} = W_i K_{\alpha\beta\gamma^x}\sigma_c - K_{\alpha\beta^x}\mu_v,$
$K_{\sigma v} = W_i K_{\alpha\beta\gamma^y}\sigma_c - K_{\alpha\beta^y}\mu_v,\quad K_{\sigma\sigma} = K_{\alpha\beta} - 2W_i(K_{\alpha\beta\gamma^x}U_c + K_{\alpha\beta\gamma^y}U_c),$
$K_{\sigma p} = 0, K_{pu} = K_{\alpha\beta^x}, K_{pv} = K_{\alpha\beta^y},\ K_{p\sigma} = 0 = K_{pp},$
$K_{\theta\theta} = RePr(K_{\alpha\beta\gamma^x}U_\beta + K_{\alpha\beta\gamma^y}V_\beta) + (S_{\alpha\beta^{xx}} + S_{\alpha\beta^{yy}}) + \rho_f K_{\alpha\beta},$
$K_{\theta u} = K_{\alpha\beta\gamma^x}\theta\gamma,\ K_{\theta v} = K_{\alpha\beta\gamma^y}\theta\gamma, K_{\sigma\theta} = K_{\theta\sigma} = 0,$
$K_{\theta p} = 0, K_{pu} = K_{\alpha\beta^x}, K_{p\theta} = 0 = K_{pp}, K_{pv} = K_{\alpha\beta^y}.$

If the percentage of the overall change compared to the previous iteration is less than the specified value, then the iteration process is terminated.

4 Numerical Results

The purpose of this work is to identify and find out the effects of stenotic and aneurysmatic artery, drag coefficient, and dimensionless numbers (Re and Wi) on blood flow for the models of (i) Newtonian (μ_n = constant, σ_v =0) (ii) Generalized Newtonian ($\mu_n = \mu(\dot\gamma)$,σ_v =0) (iii) Oldroyd-B (μ_n =constant, σ_v) (iv) Generalized Oldroyd-B ($\mu_n = \mu(\dot\gamma)$,σ_v =). All types are used to analyze the effect of the shear-thinning and viscoelastic behavior of human blood. In this paper, non-Newtonian fluids are of great interest due to blood viscoelasticity behaviour. It is found that the generalized Oldroyd-B type models are more appropriate to analyze blood flow simulations and ensure more accuracy. In the 2D stenotic and aneurysmatic models, the parabolic velocity and the extra stresses components are employed because of the viscous properties of blood for the generalized cases.

A real case study has been done [4] for endovascular treatment in the case of abdominal aortic aneurysm and renal artery stenosis with renal function and blood pressure. A cardiovascular electronic system has been used [24] to analyze the artery of aneurysms and renal stenosis. The results have shown the pressure is decreased due to the aneurysms and stenosis. In this study, the mathematical method showed that compliances of the aorta portions and renal increased with the increased rate of the aneurysmal and stenotic artery. A study of multiple aneurysms and multiple stenotic lesions in the renal artery and segmental arteries have been completed [23] for a 13-year-old boy with type I neurofibromatosis and severe hypertension.Real analysis is found [57] for a patient with behcet's disease in the presence of stenosis and aneurysm of Coronary Arteries.

Recently, a case report is found [28] for an HIV-infected 53-year-old man and they have discussed the impact of coronary artery aneurysm, ectasia, and stenosis on blood flow.

To evaluate the accuracy and confirmation of this work, we have computed a validation test with Prokop et al [45] for Newtonian (N), generalized Newtonian (GN), Oldroyd-B (OD) and generalized Oldroyd-B (GD) cases. We calculate velocity, pressure, and drag coefficients with various dimensionless numbers for the considered model. In the present numerical study, the following thermal properties and tissue [63] are used:

$0 \leq Wi \leq 1,\ 0 < Re \leq 3000, \mu_0 = 0.16Pa.s, \mu_n = 0.0036Pa.s, a = 1.23, b = 0.64, \lambda = 8.2s, \rho = 1050kg.m^{-}3, T_b = 370c, C_b = 3770(J/Kg.k), W_b = 0.5(Kg/sec.m^3),\ K = 0.5(J/s.m.k), P_f = 400, L_w = 2R, L = 0.03m, R = 3.1mm, h_s = R$ and $h_a = 3R$.

It is a very important investigation to find out the effects of Reynold numbers, Weissenberg number, stenotic and aneurysmatic artery, and drag coefficient at the stenosed wall on blood flow for the various models Newtonian (N), generalized Newtonian (GN), Oldroyd-B (OD) and generalized Oldroyd-B (GD). The comparative study of blood flow simulation is shown in Figures 8, 9 and 11 with the presence and absence of blood clots at the present model in terms of axial velocity and pressure contour lines for all cases. The blood flow characteristics have a significant change at the throat of stenosis. Figures 10, 12, 13 and 14 provide the graphical illustration of the velocity, pressure, wall shear stress and drag coefficient of blood flow. The graphical of blood flows has been shown in Figure 7 as follows, which is almost similar to the previously published work by Prokop et. al. [45].

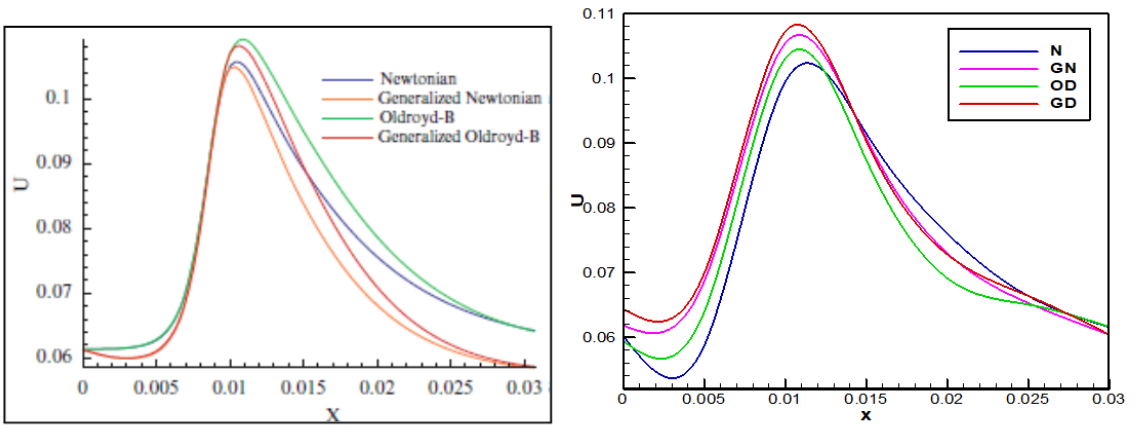

Figure 7: Contrast of velocity contour for all models with V. Prokop et al. (left) and present work (right).

4.1 Stenotic and Aneurysmatic Effects on Blood Flow

The blood flow simulation is shown in Figures 8 and 9 with the presence and absence of blood clots at bottom stenosed walls for all models. The indelible recirculation zones originate at the constriction region of the stenotic and aneurysmatic arteries for all cases. The shape of the recirculation zone is oval-like and it has been reduced at the generalized Oldroyd-B model. This recirculation is indicative of iso-blood flow at the stenotic artery. The blood shear-thinning properties are important reasons to form the recirculation zone and dominate the low-shear area of stenotic and aneurysmatic arteries. At aneurysms, the velocity contour lines are almost alike for

Newtonian and Oldroyd-B models, but little dissimilarity is found at the rest of the models. In the absence of blood clots, the blood flow simulation is presented in Figure 8 (right) for the mentioned models where the recirculation zones are found at the throat of stenosis. These recirculation zones are symbolic of regions over a significant portion of each model where the flow is moving at the same values. The recirculated area is comparable bigger at blood clotted models than non-blood clotted models for all cases. The shape of the recirculation zone is another significant influence of blood clots among the models. At aneurysm, the reversal flow regions and flow separation are found concerning to the vessel axis in the Figures 8 and 9 but greater flow separation regions are created in non-blood clot models. It is clearly visible for non-blood clot in the Figure 9, the backflow is found just behind the stenotic region and centre of the aneurysmal area. A significant disorder of blood flow has developed at dilation area for Newtonian and generalized Newtonian cases.

Figure 10 provides the corresponding effects on blood velocity numerically at the presence and absence of blood clots for all models where $Re = 1000$ and $Wi = 0.5$. It is observed that the velocity profile is almost opposite for the blood clot model and the non-blood clot model. The maximum blood velocity is found at the throat of stenosis for the non-blood clot model and the lowest value is in the blood clot model. For the existence of blood clots, the blood velocity is comparable lower to another model which leads to local viscosity increases significantly.

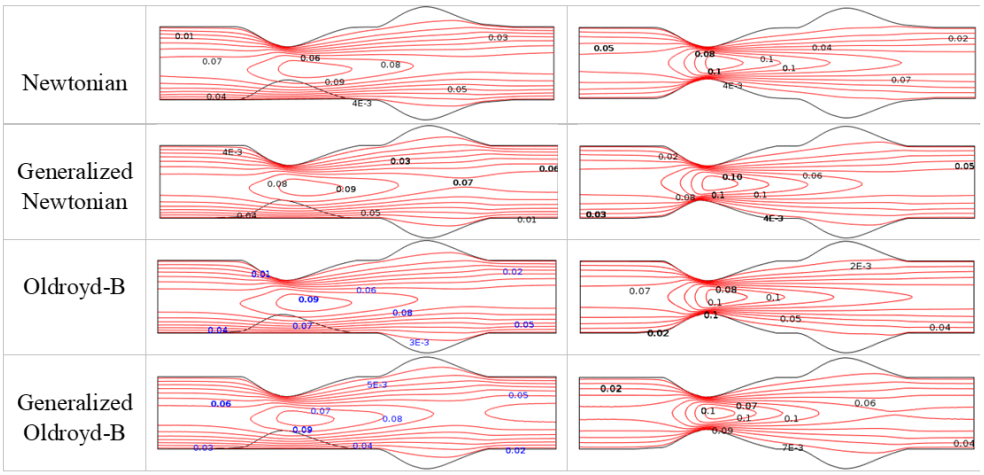

Figure 8: Velocity contour line on blood flow through stenosed and anuerysmatic vessel with blood clot (left) and without blood clot (right) at Re=1000 and Wi = 0.6.

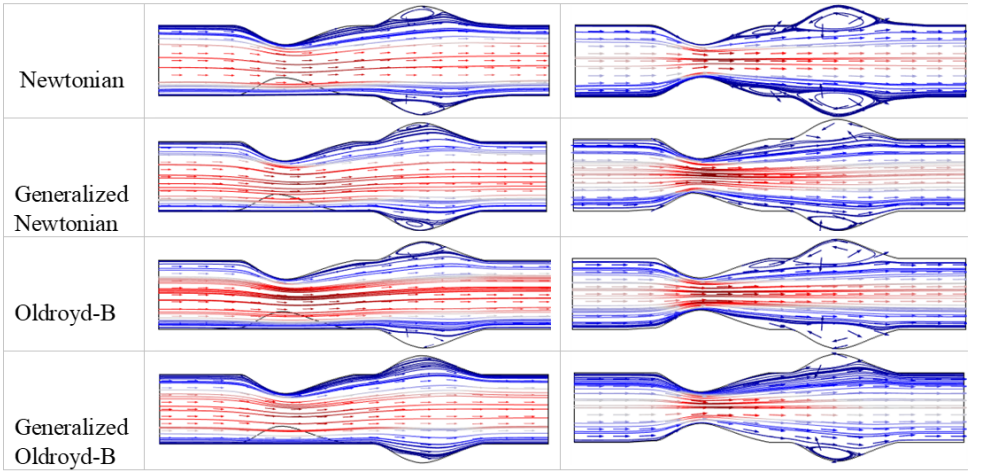

Figure 9: Vector patterns on blood flow with blood clots (left) without blood clots (right) at Re=1000 and Wi = 0.6.

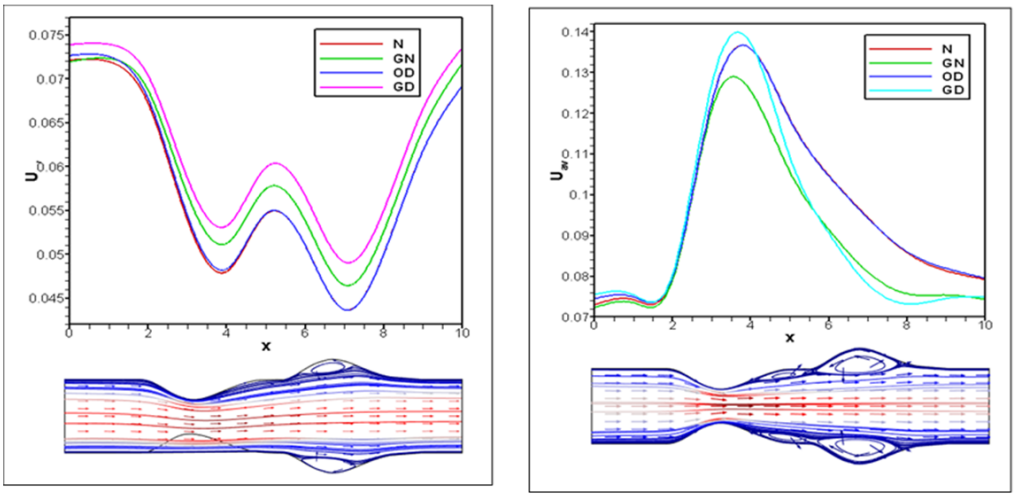

Figure 10: Comparison of velocity profile with blood clot (left) and without blood clots (right).

4.2 Stenotic and Aneurysmatic Effects on Pressure Distribution

The pressure distribution of blood flow is exhibited for all cases in Figure 11 having blood clots and without blood clots. In Figure 11 (left), the steep contour plots display the pressure gain at a minimum value at the separation point and decline gradually along the vessel axis. Due to the formation of blood clots, the pressure has peaked at the reattachment point in the stenosis region and the pressure gradient is high for all events, which is agrees with Muraki's [37] test. The pressure gradient has changed slowly and densely at clotted area. In the case of the generalized Oldroyd-B model, pressure contour lines become more compact and distort curves within a clotted area because of the shear-thinning properties of blood. The different pressure contour plots of blood flow are found in the Figure 11 (right) for all situations. The parabolic profile has developed at the throat of stenosis, and separation points are originated which leads to how the pressure has reached a minimum point. The main difference is visible between the two models at the constriction area for all models. The pressure is more dominated at stenosis regions compared to blood clot models because of blood viscosity. In the Figure 11 (right), the pressure patterns are almost alike for all models, and show the similarities at the far end of stenosis but various pressure contour plots are produced at blood-clotted models. From Figure 12, the blood pressure has decreased gradually in the presence of a blood clot and has dramatically changed for non-blood clotting cases. In the absence of blood clots, the pressure gained the lowest value at the throat of stenosis and increased after stenosis. The Newtonian fluid is faster than the non-Newtonian fluid for both cases, which leads to a minimum value at the generalized Oldroyd-B model.

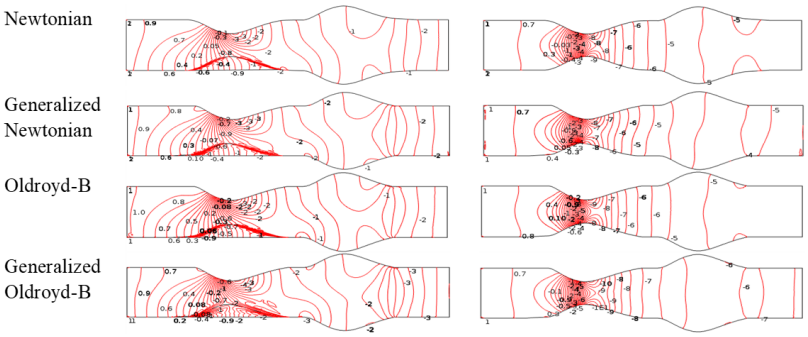

Figure 11: Pressure distribution on blood flow through stenosed and anuerysmatic vessel with blood clots (left) and without blood clots (right) at $Re = 1000$ and $Wi = 0.6$.

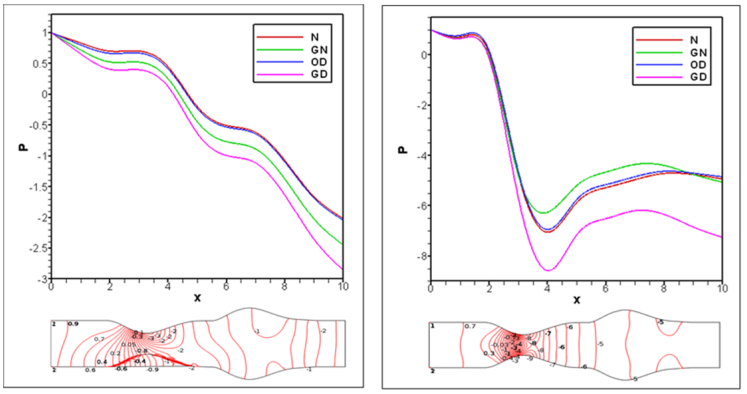

Figure 12: Comparison of pressure profile with blood clot (left) and without blood clot (right).

4.3 Drag Coefficient Effects on Blood Flow

In Figure 13, the drag coefficient (resistance) of blood flow has increased at the blood clot model and non-blood clot model. It is found that in the absence of blood clots at the stenotic area, the drag coefficient is high compared to having blood clots in a stenosis artery for Newtonians for Newtonian, Generalized Newtonian, Oldroyd-B, Generalized Oldroyd-B models with the flow rate $q = 0.1cm^3/s$. In the case of non-blood clots, the resistance of blood flow is almost the same for the Newtonian and Oldroyd-B models, but the stenotic zones have created more obstacles to blood flow at the generalized Oldroyd-B model because of viscoelastic behaviour. The hindrance of blood flow over blood lumps has increased for all cases, but the hurdle is more at a generalized model for viscosity. From Figure 14, the blood flow resistance increases with the increases of Reynold numbers, and Weissenberg numbers for all four models. The magnitude of the drag coefficient is higher for the generalized model and lower for the Oldroyd-B model with increases in the Reynold numbers. Behr et al. [8] have shown that the drag coefficient is a function of Weissenberg numbers and it increases for all cases with increases in Wi. The most significant value of the drag coefficient has originated at the generalized Oldroyd-B model in the low shear region.

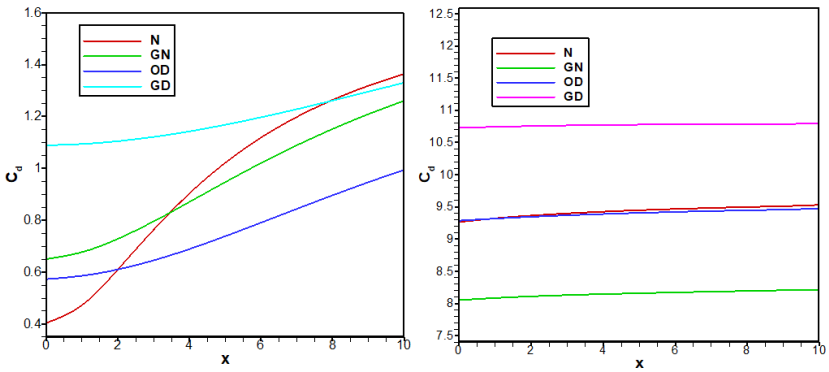

Figure 13: Drag effects of blood at bottom stenosed vessel wall with blood clots (left) and without blood clots (right) when $Re = 1000$ and $Wi = 0.6$.

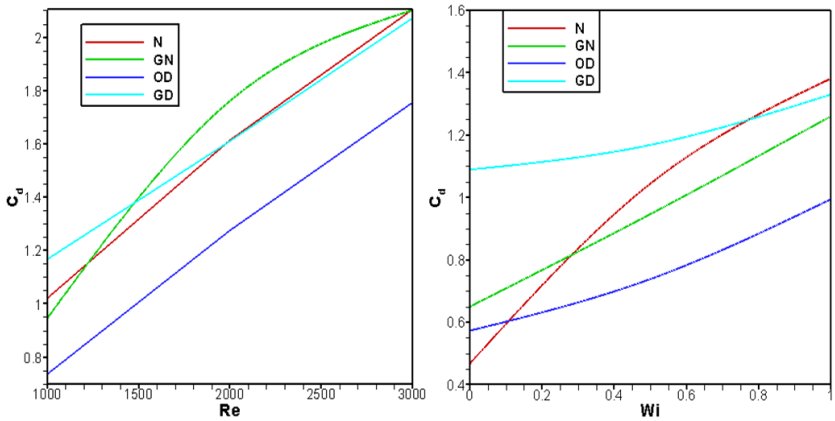

Figure 14: Drag effects of blood flow at bottom stenosed vessel wall having blood clots with respect to Re (left) and Wi (right) for all models.

5 Conclusions

In this paper, the simultaneous effects of stenosis and aneurysm in the blood clotting artery have been discussed along with the generalized models and Oldroyd B-fluid model. The finite element technique is used to simulate the physical problem. The generalized Newtonian model, Oldroyd-B models and generalized Oldroyd-B models are used to investigate blood viscosity and shear-thinning properties accurately. The change in blood flow patterns is insignificant at the blood clotting area for all models compared to the stenotic area. So, any stenotic artery indicates severe atherosclerosis diseases and creates disorder in human blood flow. Among all models, the generalized Oldroyd-B model has shown the best performance to find out blood flow variables due to the shear-thinning and viscoelasticity properties of blood. The impact of stenotic vessels, aneurysmatic arteries, blood clots, dimensionless numbers and drag coefficients are very important for blood flow analysis. In this study, it is found that the effect of stenotic and aneurysmatic artery on blood flow is significant. It is found that blood velocity and pressure have changed rapidly at the throat of stenosis for stenotic models compared to blood clots models. The efficiency and competence of the theoretical results have been discussed by numerical method using finite element techniques. Based on the above computational results, we conclude that:

1. The shear-thinning effects are related to the blood velocity and pressure that are more pronounced than the viscoelastic ones.
2. The blood flow parameters are predominant in the recirculation zones compared to the blood clot model.
3. The impact of blood clots on blood flow behavior at the hub of stenosis is a key cause in the onset of atherosclerosis diseases.
4. The effect of the drag coefficient on blood flow is more extreme in stenotic (without blood clot) arteries for all models. It is an important factor to identify arterial diseases.
5. Due to the presence of blood clots at the throat of stenosis, the recirculation zones are more elliptic for all models, and minimum velocity and maximum blood pressure are observed.
6. The impact of stenosis and aneurysm artery on blood flow leads to the severeness of arterial diseases which may be helpful in medical science.

7. Blood velocity has achieved the maximum value at the narrow cross-sectional area (centre of the stenotic artery) in the absence of blood clots and gained a minimum value at the dilated cross-sectional area with the presence of blood clots, which is theoretically authentic. Besides, we have computed blood pressure for the present model, and the result is quite agreeable with the theory for all cases.

Conflicts of Interest The authors declare no conflicts of interest.

References

[1] Comsol multiphysics 4.3a. https://cdn.comsol.com/doc/4.3a/COMSOL_ReleaseNotes.pdf. Accessed: 2020-12-18.

[2] How to read an MRI lumbar spine in 8 easy steps. https://healthcareextreme.com/how-to-read-mri-lumbar-spine-in-8-easy-steps/. Accessed: 2020-12-18.

[3] L. Achab, M. Mahfoud & S. Benhadid (2016). Numerical study of the non-Newtonian blood flow in a stenosed artery using two rheological models. *Thermal Science*, *20*(2), 449–460. https://doi.org/10.2298/TSCI130227161A.

[4] B. Agroyannis, A. Chatziioannou, D. Mourikis, N. Patsakis, K. Katsenis, S. Kalliafas, P. Dimakakos & L. Vlachos (2002). Abdominal aortic aneurysm and renal artery stenosis renal function and blood pressure before and after endovascular treatment. *Journal of Human Hypertension*, *16*(5), 367–369. https://doi.org/10.1038/sj.jhh.1001367.

[5] A. S. Alsagri, S. Nasir, T. Gul, S. Islam, K. S. Nisar, Z. Shah & I. Khan (2019). MHD thin film flow and thermal analysis of blood with CNTs nanofluid. *Coatings*, *9*(3), 175. https://doi.org/10.3390/coatings9030175.

[6] M. Anand & K. R. Rajagopal (2004). A shear-thinning viscoelastic fluid model for describing the flow of blood. *International Journal of Cardiovascular Medicine and Science*, *4*(2), 59–68.

[7] M. K. Anand & K. R. Rajagopal (2005). A model for the formation and analysis of blood clots. *Pathophysiology of Haemostasis and Thrombosis*, *34*(2-3), 109–120. https://doi.org/10.1159/000089931.

[8] M. Behr, D. Arora & M. Pasquali (2004). Stabilized finite element methods of GLS type for Oldroyd-B viscoelastic fluid. *European Congress on Computational Methods in Applied Sciences and Engineering*, *2004*, 1–16.

[9] E. Belardinelli & S. Cavalcanti (1991). A new nonlinear two-dimensional model of blood motion in tapered and elastic vessels. *Computers in Biology and Medicine*, *21*(1-2), 1–13. https://doi.org/10.1016/0010-4825(91)90030-D.

[10] M. M. Bhatti, A. Z. L. S. Riaz, S. M. & R. Ellahi (2020). Biologically inspired thermal transport on the rheology of williamson hydromagnetic nanofluid flow with convection an entropy analysis. *Journal of Thermal Analysis and Calorimetry*, *144*, 2187–2202. https://doi.org/10.1007/s10973-020-09876-5.

[11] R. B. Bird, W. E. Stewart & E. N. Lightfoot (2001). *Transport phenomena*. John Wiley & Sons, New Jersey, USA.

[12] T. Bodnar, A. Sequeira & M. Prosi (2011). On the shear-thinning and viscoelastic effects of blood flow under various flow rates. *Applied Mathematics and Computation*, *217*(11), 5055–5067. https://doi.org/10.1016/j.amc.2010.07.054.

[13] C. G. Caro, T. J. Pedley, R. C. R. Schrote & W. A. Seed (1978). *The mechanics of the circulation*. Oxford University Press, Oxford, UK.

[14] S. Cavalcanti (1995). Hemodynamics of an artery with mild stenosis. *Journal of Biomechanics*, *28*(4), 387–399. https://doi.org/10.1016/0021-9290(94)00084-h.

[15] S. Chakravarty & P. K. Mandal (2000). Two-dimensional blood flow through tapered arteries under stenotic conditions. *International Journal of Non-Linear Mechanics*, *35*(5), 779–793. https://doi.org/10.1016/S0020-7462(99)00059-1.

[16] J. L. Cronenwett, T. F. Murphy, G. B. Zelenock, W. M. Whitehouse Jr, S. M. Lindenauer, L. E. Graham L. M. nad Quint, T. M. Silver & J. C. Stanley (1985). Actuarial analysis of variables associated with rupture of small abdominal aortic aneurysms. *Surgery*, *98*(3), 472–83.

[17] P. Dechaumphai (1999). *Finite element method in engineering*. Chulalongkorn University Press, Bangkok.

[18] C. B. Ernst (1993). Abdominal aortic aneurysm. *New England Journal of Medicine*, *328*(16), 1167–1172. https://doi.org/10.1056/NEJM199304223281607.

[19] J. L. Faveroa, A. R. Secchi, N. S. M. Cardozoa & H. Jasakc (2010). Viscoelastic flow analysis using the software OpenFOAM and differential constitutive equations. *Journal of Non-Newtonian Fluid Mechanics*, *165*(23-34), 1625–1636. https://doi.org/10.1016/j.jnnfm.2010.08.010.

[20] C. P. Fetecau, S. C. & K. R. Rajagopal (2007). A note on the flow induced by a constantly accelerating plate in an Oldroyd-B fluid. *Applied Mathematical Modelling*, *31*(4), 647–654. https://doi.org/10.1016/j.apm.2005.11.032.

[21] G. P. Galdi, R. Rannacher, A. M. Robertson & S. Turek (2008). *Hemodynamical flows, analysis and simulation*. Birkhauser, Basel, Switzerland.

[22] P. Hall (1974). Unsteady viscous flow in a pipe of slowly varying cross-section. *Journal of Fluid Mechanics*, *64*(2), 209–226. https://doi.org/10.1017/S0022112074002369.

[23] M. Han, M. Enrique & M. Criado (2005). Renal artery stenosis and aneurysms associated with neurofibromatosis. *Journal of Vascular Surgery*, *41*(3), 539–543. https://doi.org/10.1016/j.jvs.2004.12.021.

[24] K. Hassani, M. Navidbakhsh & M. Rostami (2007). Modeling of the aorta artery aneurysms and renal artery stenosis using cardiovascular electronic system. *BioMedical Engineering OnLine*, *6*, 22. https://doi.org/10.1186/1475-925X-6-22.

[25] K. E. Hoque, M. Ferdows, S. T. Sawall, E. E. & M. A. Xenos (2021). Hemodynamic characteristics expose the atherosclerotic severity in coronary main arteries one-dimensional and three-dimensional approaches. *Physics of Fluids*, *33*(12), 121907. https://doi.org/10.1063/5.0069106.

[26] C. J. H. Ingoldby, R. Wujanto & J. E. Mitchell (1986). Impact of vascular surgery on community mortality from ruptured aortic aneurysms. *British Journal of Surgery*, *73*(7), 551–563. https://doi.org/10.1002/bjs.1800730711.

[27] M. Kahshan, D. Lu & A. M. Siddiqui (2019). A jeffrey fluid model for a porous-walled channel: application to flat plate dialyzer. *Scientific Reports*, *9*, 15879. https://doi.org/10.1038/s41598-019-52346-8.

[28] A. Kashyap, D. Abramov, A. Bharadwaj, M. Rabkin & D. G. Rabkin (2022). Coronary artery aneurysm, ectasia and stenosis in a 53-year-old man with HIV infection. *Journal of Surgical Case Reports*, *2022*(3), rjac056. https://doi.org/10.1093/jscr/rjac056.

[29] B. R. Kumar, G. A. Kumar & S. M. Kumar (2010). *MATLAB and its application in engineering*. Pearson Education, London.

[30] B. V. R. Kumar & K. B. Naidu (1995). Finite element analysis of nonlinear pulsatile suspension flow dynamics in blood vessels with aneurysm. *Computers in Biology and Medicine*, *25*(1), 1–20. https://doi.org/10.1016/0010-4825(95)98881-D.

[31] D. Liepsch (2002). An introduction to biofluid mechanics basic models and applications. *Journal of Biomechanics*, *35*(4), 415–435. https://doi.org/10.1016/S0021-9290(01)00185-3.

[32] Q. Long, X. Y. Ku, K. Ramnarine & P. Hoskins (2001). Numerical investigation of physiologically realistic pulsatile flow through arterial stenosis. *Journal of Biomechanics*, *34*(10), 1229–1242. https://doi.org/10.1016/S0021-9290(01)00100-2.

[33] J. Malek, J. Necas, M. Rokyta & M. Ruzicka (1996). *Weak and measure-valued solutions to evolutionary PDE's*. Chapman & Hall, New York, NY.

[34] P. K. Mandal (2005). An unsteady analysis of non-newtonian blood flow through tapered arteries with a stenosis. *International Journal of Non-Linear Mechanics*, *40*(1), 151–164. https://doi.org/10.1016/j.ijnonlinmec.2004.07.007.

[35] M. J. Manton (1971). Low Reynolds number flow in slowly varying axisymmetric tubes. *Journal of Fluid Mechanics*, *49*(3), 451–459. https://doi.org/10.1017/S0022112071002192.

[36] S. Mukhopadhyay & G. C. Layek (2011). Analysis of blood flow through a modelled artery with an aneurysm. *Applied Mathematics and Computation*, *217*(16), 6792–6801. https://doi.org/10.1016/j.amc.2010.10.011.

[37] N. Muraki (1983). Ultrasonic studies of the abdominal aorta with special reference to hemodynamic considerations on thrombus formation in the abdominal aortic aneurysm. *Journal of Japanese College Angiology*, *23*, 401–413.

[38] S. Nadeem & S. Ijaz (2015). Theoretical analysis of metallic nanoparticles on blood flow through tapered elastic artery with overlapping stenosis. *IEEE Transactions on Nanobioscience*, *14*(4), 417–428. https://doi.org/10.1109/tnb.2015.2389253.

[39] R. E. Nerem (1992). Vascular fluid mechanics, the arterial wall and arteriosclerosis. *Journal of Biomechanical Engineering*, *114*(3), 274–282. https://doi.org/10.1115/1.2891384.

[40] S. Oka (1973). Pressure development in a non-newtonian flow through a tapered tube. *Rheologica Acta*, *12*, 224–227. https://doi.org/10.1007/BF01635108.

[41] J. Oldroyd (1950). On the formulation of rheological equations of state. *Proceedings of the Royal Society A*, *200*(1063), 523–541. https://doi.org/10.1098/rspa.1950.0035.

[42] R. G. Owens & T. N. Phillips (2002). *Computational rheology*. World Scientific, Singapore.

[43] H. H. Pennes (1948). Analysis of tissue and arterial blood temperatures in the resting human forearm. *Journal of Applied Physiology*, *1*(2), 5–34. https://doi.org/10.1152/jappl.1948.1.2.93.

[44] G. Porenta, G. F. Young & T. R. Rogge (1986). A finite element model of blood flow in arteries including taper, branches and obstructions. *Journal of Biomechanical Engineering*, *108*(2), 16–167. https://doi.org/10.1115/1.3138596.

[45] V. Prokop & K. Kozel (2013). Numerical simulation of generalized newtonian and oldroyd-b fluids. In A. Cangiani, R. Davidchack, E. Georgoulis, A. Gorban, J. Levesley & M. Tretyakov (Eds.), *Numerical Mathematics and Advanced Applications 2011*, pp. 579–586. Springer, Berlin, Heidelberg. https://doi.org/10.1007/978-3-642-33134-3_61.

[46] H. T. Qi & M. Y. Xu (2007). Stokes first problem for a viscoelastic fluid with the generalized oldroyd-b model. *Acta Mechanica Sinica*, *23*, 463–469. https://doi.org/10.1007/s10409-007-0093-2.

[47] K. R. Rajagopal & A. R. Srinivasa (2011). A Gibbs-potential-based formulation for obtaining the response functions for a class of viscoelastic materials. *Proceedings of the Royal Society A*, *467*(2125), 39–58. https://doi.org/10.1098/rspa.2010.0136.

[48] C. Rajashekhar, G. Manjunatha & B. Fabian (2017). Finite element simulation of blood flow through an artery bifurcation: a mathematical model. *Malaysian Journal of Mathematical Sciences*, *11*(2), 165–179.

[49] J. N. Reddy & Gartling (2010). *Fundamentals of the finite element method in heat transfer*. CRC Press, Boca Raton, Florida.

[50] S. I. A. Salam, M. M. Bhatti, R. Zeeshan, A. A. & O. A. Beg (2019). Metachronal propulsion of a magnetised particle-fluid suspension in a ciliated channel with heat and mass transfer. *Physica Scripta*, *94*(11), 115301. https://doi.org/10.1088/1402-4896/ab207a.

[51] A. Sequeira & J. Janela (2007). An overview of some mathematical models of blood rheology. In *Pereira, M.S. (eds) A Portrait of State-of-the-Art Research at the Technical University of Lisbon*, pp. 65–87. Springer, Dordrecht.

[52] Z. Shah, A. Khan, W. Khan, M. K. Alam, S. Islam, P. Kumam & P. Thounthong (2019). Micropolar gold blood nanofluid flow and radiative heat transfer between permeable channels. *Computer Methods and Programs in Biomedicine*, *186*, 105197. https://doi.org/10.1016/j.cmpb.2019.105197.

[53] T. C. Shih, P. Yuan, W. Lin & H. S. Kou (2007). Analytical analysis of the pennes bioheat transfer equation with sinusoidal heat flux condition on skin surface. *Medical Engineering & Physics*, *29*(9), 946–953. https://doi.org/10.1016/j.medengphy.2006.10.008.

[54] A. M. Siddiqui, A. A. Farooq & M. A. Rana (2015). An investigation of non-Newtonian fluid flow due to metachronal beating of cilia in a tube. *International Journal of Biomathematics*, *8*(2), 1–23. http://dx.doi.org/10.1142/S1793524515500163.

[55] O. Smedby (1997). Do plaques grow upstream or downstream? an angiographic study in the femoral artery. *Arteriosclerosis, Thrombosis, and Vascular Biology*, *17*(5), 912–918. https://doi.org/10.1161/01.ATV.17.5.912.

[56] F. T. Smith (1979). The separation flow through a severely constricted symmetric tube. *Journal of Fluid Mechanics*, *90*(4), 725–754.

[57] H. H. Sonia, B. K., M. Sylvia, M. Faouzi, G. Habib & B. F. Mohamed (2008). Stenosis and aneurysm of coronary arteries in a patient with behçet's disease. *The Open Cardiovascular Medicine Journal*, *2*, 118–120. http://dx.doi.org/10.2174/1874192400802010118.

[58] C. Taylor & P. Hood (1973). A numerical solution of the Navier-Stokes equations using the finite element technique. *Computers & Fluids*, *1*(1), 73–100. https://doi.org/10.1016/0045-7930(73)90027-3.

[59] G. B. Thurston (1973). Frequency and shear rate dependence of viscoelasticity of blood. *Biorheology*, *10*(3), 375–381. https://doi.org/10.3233/bir-1973-10311.

[60] C. Tu, M. Deville, L. Dheur & L. Vanderschuren (1992). Finite element simulation of pulsatile flow through arterial stenosis. *Journal of Biomechanics*, *25*(10), 1141–1152. https://doi.org/10.1016/0021-9290(92)90070-H.

[61] M. N. Uddin & M. A. Alim (2017). Numerical investigation of blood flow through stenotic artery. *World Journal of Engineering Research and Technology*, *3*(6), 93–116.

[62] M. N. Uddin & M. A. Alim (2017). Numerical study of blood flow through symmetry and non-symmetric stenosis artery under various flow rates. *IOSR Journal of Dental and Medical Sciences*, *16*(6), 106–115. http://dx.doi.org/10.9790/0853-160601106115.

[63] C. Verdier (2003). Rheological properties of living materials. from cells to tissues. *Computational and Mathematical Methods in Medicine*, *5*, Article ID: 459319, 25 pages. https://doi.org/10.1080/10273360410001678083.

[64] S. Wille (1981). Pulsatile pressure and flow in an arterial aneurysm simulated in a mathematical model. *Journal of Biomedical Engineering*, *3*(2), 153–158. https://doi.org/10.1016/0141-5425(81)90010-8.

[65] W. T. Wu & M. Massoudi (2020). Recent advances in mechanics of non-Newtonian fluids. *Fluids*, *5*(10), 1. https://doi.org/10.3390/fluids5010010.

[66] A. Zaman, N. Ali, O. A. Beg & M. Sajid (2016). Unsteady two-layered blood flow through a w-shaped stenosed artery using the generalized Oldroyd-B fluid model. *The ANZIAM Journal*, *58*(1), 96–118. https://doi.org/10.1017/S1446181116000134.

[67] A. Zaman, N. Ali & M. Sajid (2016). Slip effects on unsteady non-newtonian blood flow through an inclined catheterized overlapping stenotic artery. *AIP Advances*, *6*(1), 015118. https://doi.org/10.1063/1.4941358.

[68] A. Zaman & A. A. Khan (2021). Time dependent non-Newtonian nano-fluid (blood) flow in w-shape stenosed channel; with curvature effects. *Mathematics and Computers in Simulation*, *181*, 82–97. https://doi.org/10.1016/j.matcom.2020.09.017.

[69] A. Zaman, A. A. Khan & N. Ali (2018). Modeling of unsteady non-newtonian blood flow through a stenosed artery with nanoparticles. *Journal of the Brazilian Society of Mechanical Sciences and Engineering*, *40*, 307. https://doi.org/10.1007/s40430-018-1230-5.

[70] A. Zaman, M. Sajid & N. Kousar (2018). Biomedical study of effects nanoparticles on unsteady blood (non-Newtonian) flow through a catheterized stenotic vessel. *Canadian Journal of Physics*, *97*(5), 487–497. https://doi.org/10.1139/cjp-2018-0376.

[71] L. Zhang, M. M. Bhatti, M. Marin & K. S. Mekheimer (2020). Entropy analysis on the blood flow through anisotropically tapered arteries filled with magnetic zinc-oxide (ZnO) nanoparticles. *Entropy*, *22*(10), 1070. https://doi.org/10.3390/e22101070.

[72] O. C. Zienkiewicz & R. L. Taylor (1991). *The finite element method*. McGraw-Hill, New York, NY.